Applied Thermal Engineering 260 (2025) 124873

Contents lists available at ScienceDirect

Applied Thermal Engineering

journal homepage: www.elsevier.com/locate/ate

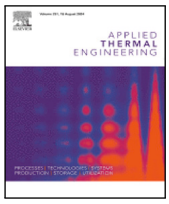

An Open-Source algorithm for automatic geometrical optimization of extruded liquid cold plates for enhanced thermal management in railway electronics

Raffaele De Rosa [a,*], Marco Bernagozzi [b], Anastasios Georgoulas [b], Luca Romagnuolo [c], Emma Frosina [c], Adolfo Senatore [a]

[a] Department of Industrial Engineering, University of Naples "Federico II", Via Claudio 21, 80125 Napoli (NA), Italy
[b] Advanced Engineering Centre, University of Brighton, Brighton, UK
[c] Department of Engineering, University of Sannio, Piazza Roma 21, 82100 Benevento (BN), Italy

ARTICLE INFO

Keywords:
Liquid Cold Plate (LCP)
OpenFOAM
Parametric simulation
Extruded LCP
Railway electronics

ABSTRACT

This paper presents the development and application of an optimization algorithm for determining the geometric parameters of an extruded Liquid Cold Plate (LCP) with internally finned channels. The entire workflow operates within a fully open-source environment, offering a comprehensive and accessible solution for optimizing LCP geometric parameters for efficient thermal management in railway power electronics as well as other industrial applications. In particular, the aim is to minimize the maximum temperature and the temperature gradient at the interface between the LCP and an electronic device for electric trains that dissipates heat. The algorithm explores a defined range of geometric parameters and automatically generates combinations and performs Computational Fluid Dynamics (CFD) simulations, using the open-source C++ toolbox OpenFOAM. Implemented in a bash script, the algorithm not only automates the simulation process but also provides a geometry of the LCP that is easy to manufacture and cost-effective. The correct value of parameters, such as the distance between the fins bottom surface and the channel base (gap), along with others, has shown a significant impact, leading to a reduction in both the maximum interface temperature (8 K) and the temperature gradient (25 K/m) within the system.

1. Introduction

In the field of railway power electronics, the efficient design of cooling systems is crucial to ensure the proper operation and durability of electronic components such as traction inverters, converters, power supply units, and other propulsion system elements [1–5]. These components generate significant amounts of heat during their normal operation, and Liquid Cold Plates are often chosen as technical solution to maintain the temperature of these components below acceptable threshold values, preventing overheating and potential damage. Given the pivotal role of these devices, literature abounds with various methods aimed at optimizing their performance. Different approaches have been explored to enhance the efficiency, thermal conductivity, and overall effectiveness of LCPs, proposing optimization methods that include considerations such as material selection, control strategies and fluid dynamics [6–8]. Moreover, a significant focus has been placed on geometric design considerations. Researchers recognize that the physical structure and layout of LCPs play a critical part in determining their heat dissipation capabilities. Various studies focus on the optimization of LCP geometry, exploring factors such as channel configurations, fin arrangements, and overall plate design [9–11], contributing to the advancement of sustainable and reliable transportation systems.

Many optimization approaches utilize the Solid Isotropic Material with Penalization (SIMP) method [12] to determine the optimal distribution of material within the design domain. This method helps to identify regions where material is needed and where voids can be present, using a design variable, γ, that ranges between 0 and 1, where $\gamma = 0$ corresponds to the solid domain, and $\gamma = 1$ represents the fluid domain. Building upon this methodology, Wang et al. [13] implemented secondary shape optimization of topological boundaries using Bezier curves to enhance cold plate heat dissipation. The algorithm adjusts coefficients and control points as design variables, resulting in improved temperature and velocity distributions. Chen et al. [14] compared Topology Optimization Cold Plate (TCP) structures generated using the SIMP method with two specific types of LCPs, the

* Corresponding author.
E-mail address: raffaele.derosa4@unina.it (R. De Rosa).

https://doi.org/10.1016/j.applthermaleng.2024.124873
Received 19 March 2024; Received in revised form 27 July 2024; Accepted 7 November 2024
Available online 22 November 2024

Nomenclature

Symbols

$\|\nabla T\|$	Temperature gradient magnitude (K/m)
A	Area of the cross-section (m^2)
a	Channel width between two fins (mm)
b	Fin width (mm)
c	Gap (mm)
c_p	Specific heat at constant pressure (J/(kg K))
c_v	Specific heat at constant volume (J/(kg K))
D_h	Hydraulic diameter (m)
e	Specific total energy per unit mass (J/kg)
g_j	Components of gravitational acceleration along the j direction (J/m^2)
h	Enthalpy (J/kg)
h_t	Convective heat transfer coefficient ($W/(m^2 K)$)
k	Thermal conductivity (W/(mK))
ke	Turbulent kinetic energy (J/kg)
L	Length of the duct (m)
l	Fin length (mm)
n	Number of fins
P	Perimeter of the cross-section (m)
p_{out}	Fluid outlet pressure (Pa)
p_{rgh}	Pressure minus the hydrostatic pressure (Pa)
Q	Volumetric flow rate (L/min)
q_i	Heat flux (J/m^2)
q_{ti}	Turbulent heat flux (J/m^2)
r	Heat source term (J/kg)
Rad	Heat source by radiation (J/)
S_{p_i}	Surface on which is distributed the thermal power in the simplified model (m^2)
S_{top_i}	Surface on which is distributed the thermal power in the entire LCP (m^2)
t	Time (s)
T_P	Thermal power (W)
T_{in}	Fluid inlet temperature (K)
T_{max}	Maximum temperature (K)
v	Velocity of the coolant (m/s)
v_i	Componet of velocity along the i direction (m/s)
v_j	Componet of velocity along the j direction (m/s)
v_{ri}	Componet of relative velocity along the i direction (m/s)
v_{rj}	Componet of relative velocity along the j direction (m/s)
x_j	Spatial coordinates (m)

Greek Symbols

α	Thermal diffusivity (m^2/s)
α_I	Type I error
Δp	Pressure drop (Pa)
ϵ_{ijk}	Levi-Civita symbol
γ	Design variable
λ	Friction factor
μ	Dynamic viscosity (Pa s)
ω_i	Angular velocity vector
ρ	Density (kg/m^3)
τ_{ij}	Component of the stress tensor (Pa)
$\tau_{t_{ij}}$	Component of the turbulent stress tensor (Pa)

Abbreviations

$\langle x^2 \rangle$	Mean square
$\sum x^2$	Sum of squares
$ANOVA$	Analysis of Variance
CFD	Computational Fluid Dynamics
Df	Degree of freedom
LCP	Liquid Cold Plate
$NSGA-II$	Non-dominated Sorting Genetic Algorithm II
PEC	Performance Evaluation Criteria
PSO	Parametric shape optimization
RCP	Rectangular-Channel Cold Plate
RSM	Response Surface Method
SCP	Serpentine-Channel Cold Plate
$SIMP$	Solid Isotropic Material with Penalization
TCP	Topology Optimization Cold Plate

Rectangular-Channel Cold Plate (RCP) and the Serpentine-Channel Cold Plate (SCP). The comparison is conducted under the condition of an equal fluid domain volume fraction. They found that the utilization of TCP leads to a reduction in the maximum temperature, temperature difference, and temperature standard deviation of the battery. Sun et al. [15] introduced a novel two-solid topology optimization method for conjugate heat transfer using the SIMP approach. Optimization outcomes indicated that employing staggered multiple inlets and outlets enhances heat transfer effectiveness compared to a single distribution. Additionally, the optimized models demonstrate superior performance over conventional rectangular flow channels, leading to a reduction in both average temperature and root mean square temperature. The same authors in [16] optimized heat sink designs, featuring a detached inlet section and free-form solid fins at the bottom, outperforming pin fin designs. The numerical tests demonstrate superior efficiency, lower pressure drop, and enhanced thermal performance across varying flow rates for the topology-optimized heat sinks.

The Non-dominated Sorting Genetic Algorithm II (NSGA-II) algorithm is also employed to optimize the performances of LCPs. This is a multi-objective optimization algorithm widely used for solving optimization problems with multiple conflicting objectives [17–20]. Tian et al. [21] employed this method to minimize the average temperature and root mean square temperature of the top and bottom surfaces of an LCP. Fan et al. [22] optimized a novel liquid-cooled thermal dissipation system with double-layered dendritic channels using NSGA-II.

Statistical methods like Response Surface Method (RSM) or ANOVA (Analysis of Variance) are extensively used to optimize LCPs. Wei et al. [23] integrated NSGA II and ANOVA to explore and enhance the heat transfer and flow resistance performance of liquid cold plates featuring serpentine channels. Kılıç et al. [24] designed and optimized a cooling plate for a lithium-ion battery pack using Taguchi–grey relational analysis. They established an empirical correlation to predict the Nusselt number for three different coolants under various geometric conditions. Zuo et al. [25] utilized a combination of RSM and NSGA-II to optimize a multi-channel cold plate under intermittent pulsating flow focusing on the average heat transfer coefficient and the energy consumption.

The various optimization methods previously discussed [21,26–28] offer significant benefits, improving temperature management and

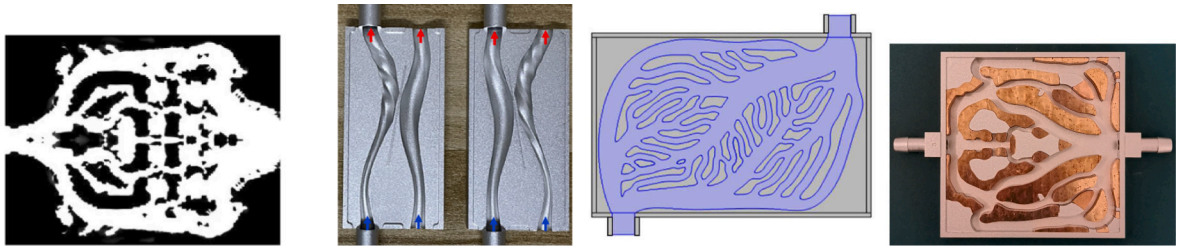

Fig. 1. Examples of optimized LCP designs (a) [27], (b) [28], (c) [14] (d) [15].

reducing pressure drops. However, the resulting optimized geometries, shown in Fig. 1, can present challenges in practical industrial applications, with complexities in manufacturing and potential prohibitive cost implications, especially for the railway applications where LCPs have considerable size.

In light of this, achieving a balance between optimal performance and feasibility is crucial in ensuring the successful implementation of these advanced optimization approaches in industrial contexts. When the general design of the LCP is fixed, this equilibrium can be realized through the parametric shape optimization [29,30]. In this process, the shape is parameterized and specific features of the design, such as dimensions, angles, or contours, are expressed as variables.

The present investigation presents a new Parametric Shape Optimization (PSO) algorithm, based on an Computational Fluid Dynamics (CFD) through a fully open-source approach, for a LCP with internally finned channels. The geometry with straight channels between the plate fins contribute to a reduction in energy consumption required to drive the flow. Moreover, finned plates can be easily manufactured using machining techniques such as milling [16] and extrusion [11], as shown in Fig. 2. In more detail, a parametric analysis was conducted to achieve hydraulic equivalence (pressure drop) among all generated configurations by varying the selected geometric parameters. In many prior works [31–34], various LCP models deriving from different combinations of geometric parameters were compared by keeping constant boundary conditions such as thermal power, inlet flow rate, or velocity, but the hydraulic equivalence was not preserved. This approach can lead to non-comparable results in terms of thermal conditions, potentially resulting in erroneous conclusions. For instance, Hadad et al. [31], demonstrated that, with the same inlet flow rate, an increase of the fin length of an LCP leads to a higher maximum temperature. This result could be misinterpreted, as it is commonly established that the temperature decreases with the increase in total convective surface area corresponding to the length of the fin [35]. This occurs because, with the same flow rate, models with shorter fins have a smaller hydraulic diameter (D_h) and this will result in higher fluid velocities and consequently a higher convective heat transfer coefficient (h_t), conversely, a longer fin results in a higher D_h that leads to lower fluid velocity and a lower h_t [36]. However, when a LCP is integrated in an hydraulic circuit in place of another, this typically alters the operating point of the entire system, thus changing the boundary conditions on the LCP itself. The need to maintain constant the operating conditions during a parametric optimization study of a device is, instead, well known to Fernandes et al. [37]. These authors have indeed conducted two parametric studies aimed at minimizing the thermal resistance of an LCP, while keeping either the flow rate or the pump power constant. However, a study where both conditions are simultaneously kept constant is missing. This is the reason why the two parametric studies by Fernandes et al. yield different results. Moreover, some performance evaluation criteria (PEC) have been developed for evaluating the performance of heat exchangers [38]. The most used criteria are based on the entropy production theorem [39] and can be used depending on the specific objective function and constraints of the optimization. In general, three cases are defined [40]: (1) reduced heat transfer surface for equal pumping power and heat duty; (2) increased ratio of thermal power to temperature unit for equal pumping power and fixed total lenght of exchanger tubing and (3) reduced pumping power for equal heat duty and total length of exchanger tubing.

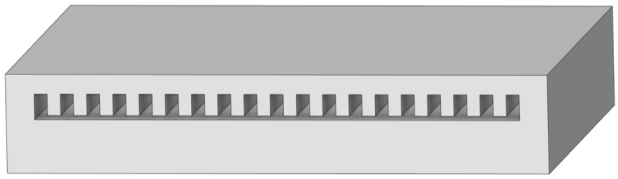

Fig. 2. Extruded part of an internally finned LCP.

In this work, the selected approach for parametric analysis, as detailed in Section 2, does not fall into any of the three previous cases because it compares models that are hydraulically equivalent and thus, as said, when integrated into the same hydraulic circuit, they work at the same operating point of mass flow rate and total pressure drop $Q - \Delta p$. In this way, unlike the previously defined PEC, conditions of equal flow rate and pump power are simultaneously satisfied making it more meaningful to compare the different maximum temperatures of the various for all the LCP configurations , and ,favouring the so-called *isointegration* conditions can be favoured. In the railway sector, maintaining isointegration is crucial when enhancing the LCP device while ensuring it remains interchangeable with the previous version. This approach prevents any imbalance in the hydraulic circuit where multiple elements, old and new, are arranged in parallel.

2. Materials and methods

As it is depicted in Fig. 3, the focus of this investigation is a LCP section with a length of $L = 100\,\text{mm}$, on top of which, an electronic device is mounted generating a thermal power $T_p = 2000\,\text{W}$ that needs to be dissipated. The system operates with a flow rate $Q = 38\,\text{L/min}$ and a pressure drop $\Delta p = 1.3 \times 10^3\,\text{Pa}$, while the liquid coolant is a mixture of water 60% and glycol 40%. In particular, the focus of this study is the internally finned U-shaped channel of the LCP, primarily fabricated through extrusion. The key aspect targeted for optimization pertains to the cross-sectional profile of the extruded part of the LCP, presenting itself as a channel with fins on the upper section.

The geometric parameters, as depicted in Fig. 4, are: a - the channel width between two fins, b - the fin width, c - the distance between the fin bottom surface and the channel base, n - the number of channels, l - the fin length.

The CFD model used for the investigation takes advantage of the geometric symmetry of the channels and reduced representative model is employed to minimize the required computational cost. In particular, only the section of the LCP illustrated in Fig. 3b is modelled, composed of two fins, a central channel, and two side semi-channels.

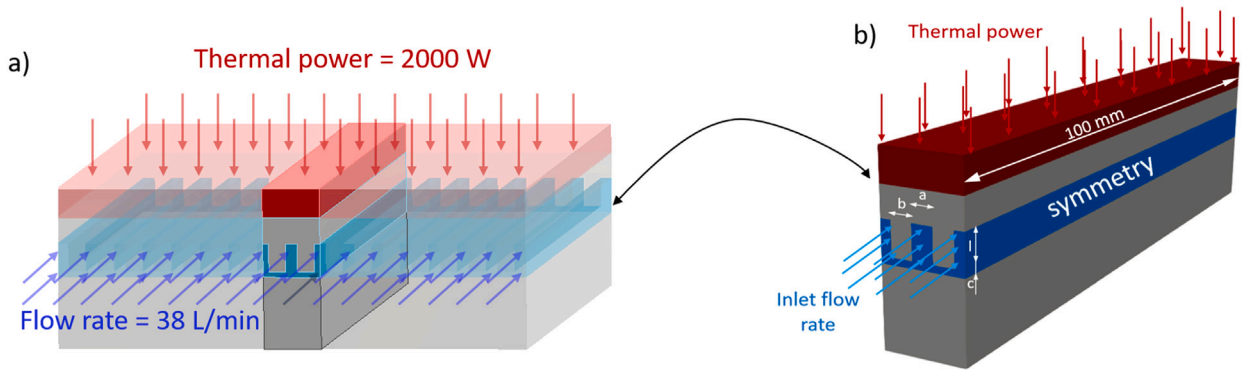

Fig. 3. (a) Extruded LCP, (b) CFD simplified model.

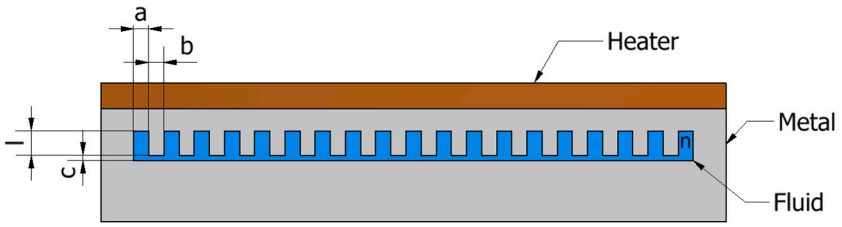

Fig. 4. Geometric parameters: a - Channel width between two fins, b - Fin width, c - Distance between the fin bottom surface and the channel base, n - Number of channels, l - Fin length.

In an effort to mitigate computational complexity during this initial optimization phase, the fins are parameterized with a rectangular configuration, avoiding the presence of fillets and rounded features. Moreover, in order to maintain hydraulic equivalence, the Darcy-Weisbach formula [41] has been adopted:

$$\Delta p = \frac{\lambda \rho L}{2} \frac{v^2}{D_h} \tag{1}$$

where, D_h is the hydraulic diameter; λ is the friction factor, a dimensionless quantity, used in the Darcy–Weisbach equation for the description of friction losses in pipe flow, that depends on the Reynolds number and the relative roughness of the inner surface of the duct; L is the length of the duct; ρ is the density of the coolant; v is the velocity of the coolant. Therefore, when incorporated into the same hydraulic circuit, all geometric configurations exhibit identical volumetric flow rates and pressure drops, providing comparable outcomes for the resulting heat transfer characteristics.

By representing the velocity v as a function of the volumetric flow rate Q and the area of the cross-sectional profile A, $v = Q/A$, it becomes feasible to establish a geometric constraint equation (Eq. (2)) that relates the wet perimeter P and the area A in a manner that ensures a similar pressure drop Δp for the same volumetric flow rate Q:

$$\Delta p = \frac{\lambda \rho L}{8} Q^2 \frac{P}{A^3} \tag{2}$$

Considering ρ and λ constant and fixing L and Q, it is evident that, the only parameter upon which Δp depends is the ratio P/A^3. This ratio, with reference to Fig. 4, can be expressed as a function of the geometric parameters of the extruded channel:

$$P/A^3 = \frac{2(an + bn - b + c + ln)}{(anl + anc + bnc - bc)^3}. \tag{3}$$

It should be noted that the hydraulic diameter formula is effective for pipes or flows with simple geometries such as circles or rectangles [42]. Therefore, keeping the parameter P/A^3 constant may still result in models with slightly different pressure drops.

Once this constraint is defined, the optimization of the LCP shape unfolds through the stages outlined in Fig. 5.

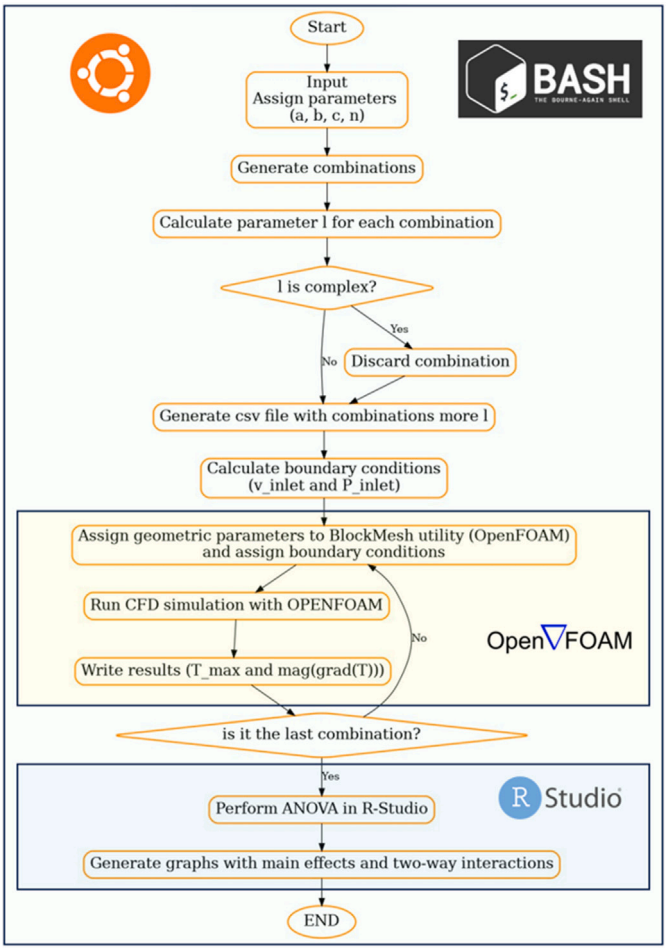

Fig. 5. Flowchart optimization algorithm.

Table 1
Independent parameters combinations.

Parameter	Level 1	Level 2	Level 3	Level 4	Level 5	Level 6	Level 7
a [mm]	2	2.5	3	3.5	4	4.5	5
b [mm]	2	2.5	3	3.5	4	4.5	5
c [mm]	0.5	1	1.5	2	2.5		
n	17	18	19	20	21		

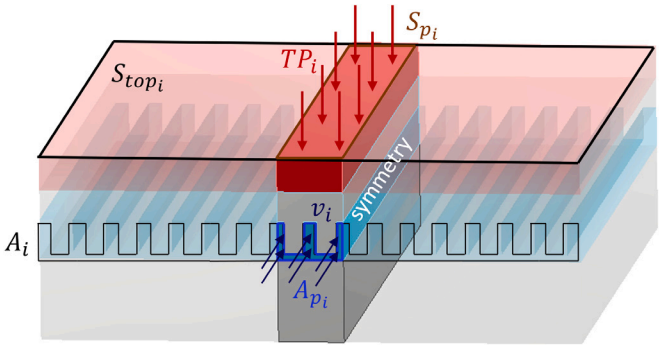

Fig. 6. Boundary condition for the simplified CFD model.

The first step is the assignment of geometric parameters, as shown in Table 1, in which seven levels for the parameters a and b and five levels for the parameters c and n are assigned.

Combining all parameters results in $7^2 + 5^2 = 1225$ sets. For each set of the parameters, the value of the parameter l is calculated using Eq. (3) in which a, b, c and n are the independent variables, l is the dependent variable and P/A^3 is fixed at 7.02×10^9 m^{-5}, in order to achieve a flow rate $Q = 38$ L/min and a pressure drop $\Delta p = 1.3 \times 10^3$ Pa (from Eq. (2)), that correspond to the system imposed operating conditions. The calculated parameter l is added to the set of geometric parameters, while the parameter sets resulting in a complex l are discarded.[1] At this stage, for each ith combination of parameters, appropriate boundary conditions are calculated and assigned to the simplified CFD model, so that they correspond to the actual boundary conditions of the entire LCP (Fig. 6).

More specifically, the thermal power for the ith combination T_{p_i}, modelled as a volumetric heat source in the entire iron domain, is computed as:

$$T_{P_i} = \frac{S_{P_i}}{S_{\text{top}_i}} T_P \tag{4}$$

where S_{top_i}, as shown in Fig. 6, is the surface on which the thermal power T_P is distributed in the actual LCP and S_{P_i} is the surface on which the thermal power of the simplified (reduced) model is distributed.

The inlet fluid velocity for the ith combination v_i is computed as:

$$v_i = \frac{Q}{A_i} \tag{5}$$

where A_i is the channel cross-sectional area of the LCP for the ith combination of parameters.

The other boundary conditions assigned to the model are: *symmetry* for the outer lateral vertical boundaries; *zero gradient* for the front and back surfaces of the solid regions; zero gradient for the bottom surface of the Aluminium bottom region; a constant fluid inlet temperature of $T_{\text{in}} = 333$ K, and a constant fluid outlet pressure of $p_{\text{out}} = 0$ Pa. To model the heat transfer at all coupled walls the boundary condition *turbulentTemperatureCoupledBaffleMixed* is used. This boundary condition represents heat transfer through the solid wall as expressed by Fourier's law [43]. Upon defining boundary conditions for each parameter combination, a conjugate heat transfer simulation is run using OpenFOAM 9. Initially, geometric parameters are assigned to the parametric structured mesh implemented in the *blockMesh* dictionary, employing nineteen blocks (Fig. 7) interconnected through the *mergePatchPairs* function. The mesh independence analysis, depicted in Fig. 8, aims to ascertain the optimal number of cells required for the simulation. The optimal mesh size for each domain includes: *Heater* mesh size of 1.5 mm, *Upper Metal* mesh size of 0.75 mm, *Fluid* mesh size of 0.375 mm, *Bottom Metal* mesh size of 1.5 mm, and a total of 320×10^3 cells.

The solver used for simulating conjugate heat transfer in the multi-region system is *chtMultiRegionFoam* [43] in which the well-known compressible Navier Stokes equation [44] are solved for the fluid regions (Eqs. (6)–(9)):

$$\frac{\partial \rho}{\partial t} + \frac{\partial \rho v_j}{\partial x_j} = 0 \tag{6}$$

$$\frac{\partial(\rho v_i)}{\partial t} + \frac{\partial}{\partial x_j}\left(\rho v_{rj} v_i\right) + \rho \epsilon_{ijk} \omega_i v_j = -\frac{\partial p_{rgh}}{\partial x_i} - \frac{\partial \rho g_j x_j}{\partial x_i} + \frac{\partial}{\partial x_j}\left(\tau_{ij} + \tau_{t_{ij}}\right) \tag{7}$$

$$\frac{\partial(\rho e)}{\partial t} + \frac{\partial}{\partial x_j}\left(\rho v_j e\right) + \frac{\partial(\rho k e)}{\partial t} + \frac{\partial}{\partial x_j}\left(\rho v_j k e\right) = -\frac{\partial(q_i + q_{ti})}{\partial x_i} + \rho r + Rad - \frac{\partial p v_j}{\partial x_i} - \rho g_j v_j + \frac{\partial}{\partial x_j}\left(\tau_{ij} v_i\right) \tag{8}$$

$$\frac{\partial \rho}{\partial t} = \frac{\partial \rho^*}{\partial t} + \psi \frac{\partial p'_{rgh}}{\partial t} \tag{9}$$

and the solid region (Eq. (10)):

$$\frac{\partial(\rho h)}{\partial t} = \frac{\partial}{\partial x_j}\left(\alpha \frac{\partial h}{\partial x_j}\right) \tag{10}$$

The thermo-physical properties of the regions are provided in Table 2.

The results of the simulations in terms of maximum temperature T_{max} and temperature gradient magnitude $|\ \nabla \mathbf{T}\ |$ at the interface between the *Heater* and *Upper Metal*, as presented in Section 3, are analysed through the ANOVA in order to assess the main effects and two-way interactions. The automation of all the tasks described earlier is performed through a Bash script and it lasts about 170 h for 1069[2] cases simulated using 12 cores of an Intel Xeon CPU E5-2640 v2 2.00 GHz processor with RAM DDR192 GB. Once the parameter matrix for individual cases is generated, the script copies the *template* folder, containing the CFD model, for each case. Subsequently, it assigns the geometric parameters and the boundary conditions, initiates the CFD simulation and records the results in a *csv* file.

3. Results and discussion

Table 3 summarizes the analysis of variance for the LCP maximum temperature, performed on the open source software R-Studio [45]. All single factors and two-way interactions, except for the interaction *b-n*, are found to be significant because the *p-value* [46] is under the type I error $\alpha_I = 0.005$ [47] but, by plotting the marginal means of the maximum temperature in Fig. 9, it is evident that the single factor with the greatest influence is the *gap* (c). As the gap increases, the temperature rises more than linearly. This is due to the fact that the effective section for cooling is the area between the fins. If the gap increases, this area decreases to maintain a constant P/A^3 ratio. The effects of b and n show similar linear trends; T_{max} decreases with their increase. The maximum temperature as a function of a exhibits a non-monotonic trend, indeed,

[1] Complex values of l correspond to the case in which the fin is in interference with the lower side of the cross-sectional area.

[2] The number of cases equals the total combinations of parameters minus the cases where l is complex ($7^2 \times 5^2 - l\_is\_complex$.)

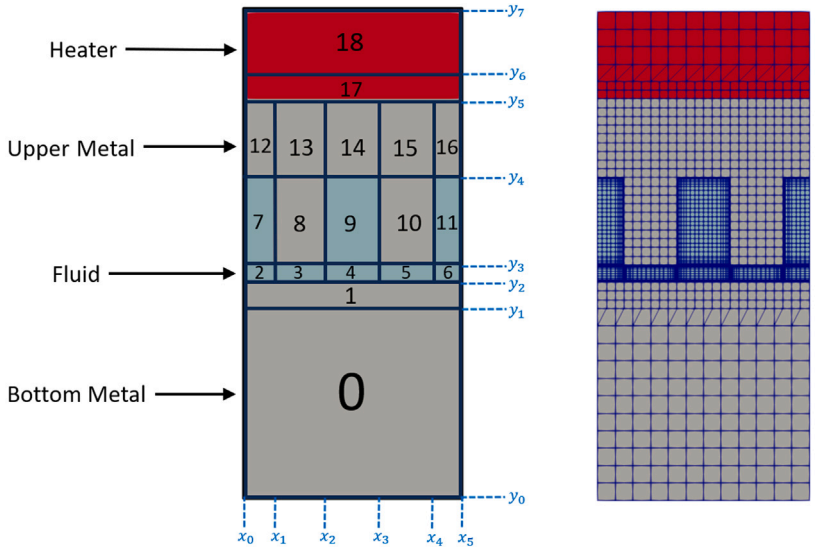

Fig. 7. Structure of the parametric mesh implemented in the *BlockMesh* dictionary.

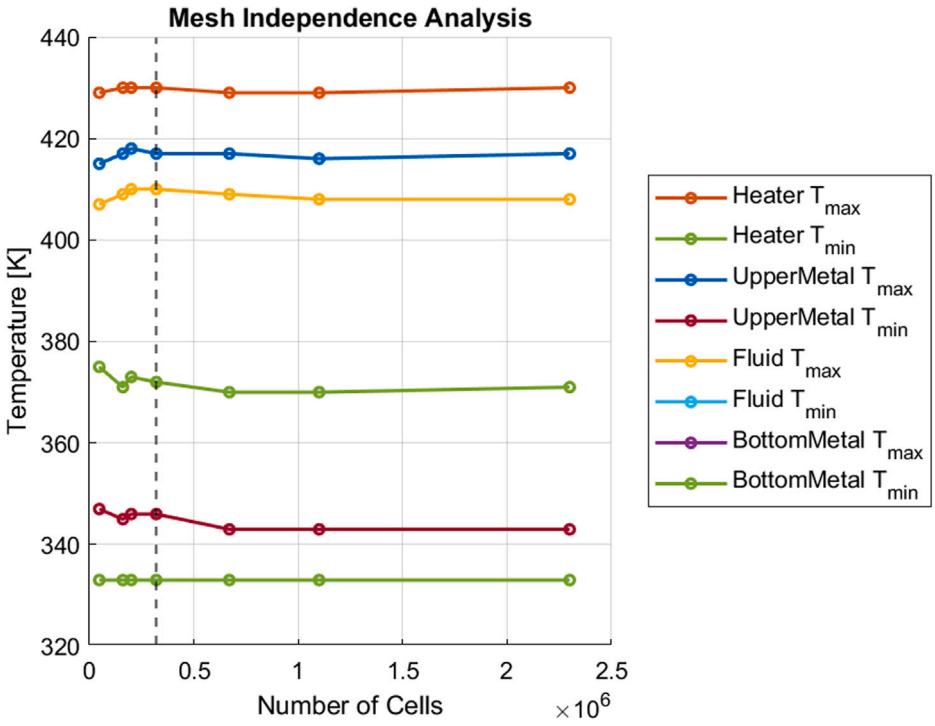

Fig. 8. Mesh independence analysis.

Table 2
Thermo-physical properties of the regions.

Region	Material	ρ [$\frac{kg}{m^3}$]	k [$\frac{W}{m\ K}$]	c_v [$\frac{J}{kg\ K}$]	c_p [$\frac{J}{kg\ K}$]	μ [Pa s]
Heater	Iron	8000	80	450		
Upper metal	Aluminium	2700	200	900		
Fluid	Water 60% - Antifrogen 40%	1027	0.445		3640	10.47×10^{-6}
Bottom metal	Aluminium	2700	200	900		

for $a^* = 3.5$ mm, a temperature peak is obtained; however, for lower values of a^*, the temperature decreases significantly, while for higher values, the temperature decreases slightly. As for the interactions, shown in Fig. 10, the one between c and n appears to be the most significant. From the graph in Fig. 10(f), it is observed that for low values of c the factor n is highly significant, while for high values of c the factor n becomes non-significant.

Table 4 summarizes the analysis of variance for the magnitude of the temperature gradient. Also in this case all single factors (see Fig. 11) and two-way interactions (see Fig. 12) are found to be significant. In this case, plots on the marginal means of the single factors | $\nabla \mathbf{T}$ |, in

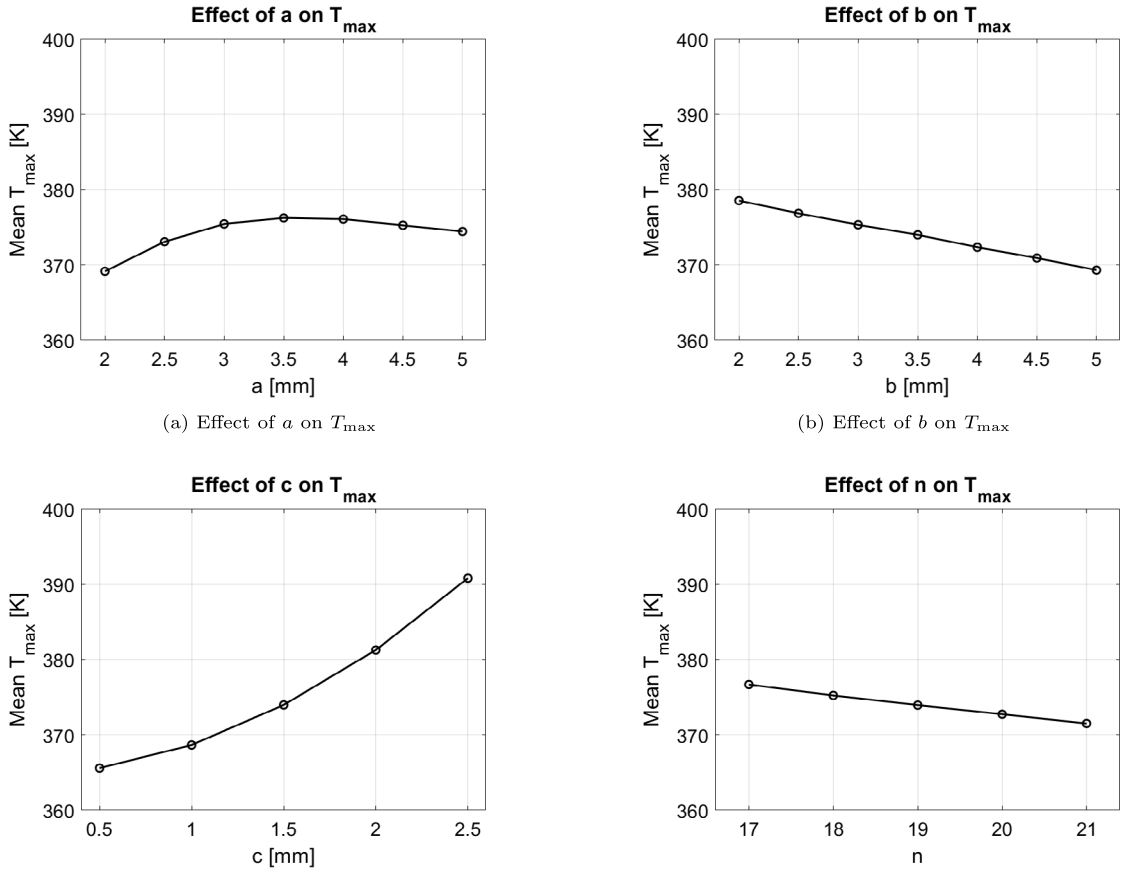

(a) Effect of a on $T_{\max}$

(b) Effect of b on $T_{\max}$

(c) Effect of c on $T_{\max}$

(d) Effect of n on $T_{\max}$

Fig. 9. Effects of single factors on the maximum temperature $T_{\max}$.

Table 3
ANOVA on the T_{max}. Factor, degree of freedom, sum of squares, mean square, Fisher's test statistic, p-value.

Factor	Df	$\sum x^2$	$\langle x^2 \rangle$	F value	p-value
a	6	6160	1027	1279.147	<2e−16
b	6	9364	1561	1944.591	<2e−16
c	4	68 642	17 160	21 382.056	<2e−16
n	4	1409	352	439.020	<2e−16
$a:b$	36	431	12	14.930	<2e−16
$a:c$	24	1276	53	66.228	<2e−16
$a:n$	24	148	6	7.669	<2e−16
$b:c$	24	1437	60	74.623	<2e−16
$b:n$	24	38	2	1.994	0.00317
$c:n$	16	497	31	38.722	<2e−16
Redsiduals	900	722	1		

Table 4
ANOVA on the $|\nabla \mathbf{T}|$. Factor, degree of freedom, sum of squares, mean square, Fisher's test statistic, p-value.

Factor	Df	$\sum x^2$	$\langle x^2 \rangle$	F value	p-value
a	6	13 742 450	2 290 408	21 777.34	<2e−16
b	6	19 767 022	3 294 504	31 324.34	<2e−16
c	4	1 542 418	385 604	3666.35	<2e−16
n	4	4 670 470	1 167 617	11 101.78	<2e−16
$a:b$	36	1 421 735	39 493	375.50	<2e−16
$a:c$	24	59 117	2463	23.42	<2e−16
$a:n$	24	78 299	3262	31.02	<2e−16
$b:c$	24	43 021	1793	17.04	<2e−16
$b:n$	24	114 253	4761	45.26	<2e−16
$c:n$	16	20 144	1259	11.97	<2e−16
Redsiduals	900	94 657	105		

Fig. 11, show all monotonic trends, particularly the plots of factors a and b exhibit steeper slopes. This means that a greater width of the channels and fins leads to a decrease in thermal gradient. Also, an increase in the number of fins (n) contributes, albeit more mildly, to reducing the thermal gradient. On the contrary, an increase in the factor c causes an increase in the magnitude of the temperature gradient. From these results, an optimized geometry has been obtained, which application is detailed in Section 3.1.

3.1. Comparison between a reference LCP and an optimized one

A comparison is performed between a reference LCP, characterized by: $a = 3$ mm, $b = 3$ mm; $c = 1$ mm, $n = 19$, and $l = 4.85$ mm, and an optimized one with the same external dimensions, characterized by $a = 2$ mm, $b = 3$ mm, $c = 0.5$ mm, $n = 19$, and $l = 10.2$ mm. The results are summarized in Table 5. In particular, Fig. 13 highlights a decrease of maximum interface temperature equal to 8 K. This improvement is primarily due to the decrease of parameter c from 1 mm to 0.5 mm, which in turn, to maintain hydraulic congruence, leads to an increase in the dependent variable l from 4.85 mm to 10.2 mm. As a consequence, there is an increase in the heat exchange surface area that leads to a lower maximum interface temperature. The decrease of parameter a from 3 mm to 2 mm and the increase of parameter b from 3 mm to 4 mm also contribute to a performance enhancement. Parameter n, on the other hand, remains constant to maintain the same external dimensions of the LCP.

Also, the temperature gradient in the LCP is slightly decreased, as shown in Fig. 14. Indeed, referring to the trends in Fig. 11, it can be observed that the decrease in a and the increase in b cause two opposite effects that balance each other out, while the decrease in c reduces the magnitude of the gradient.

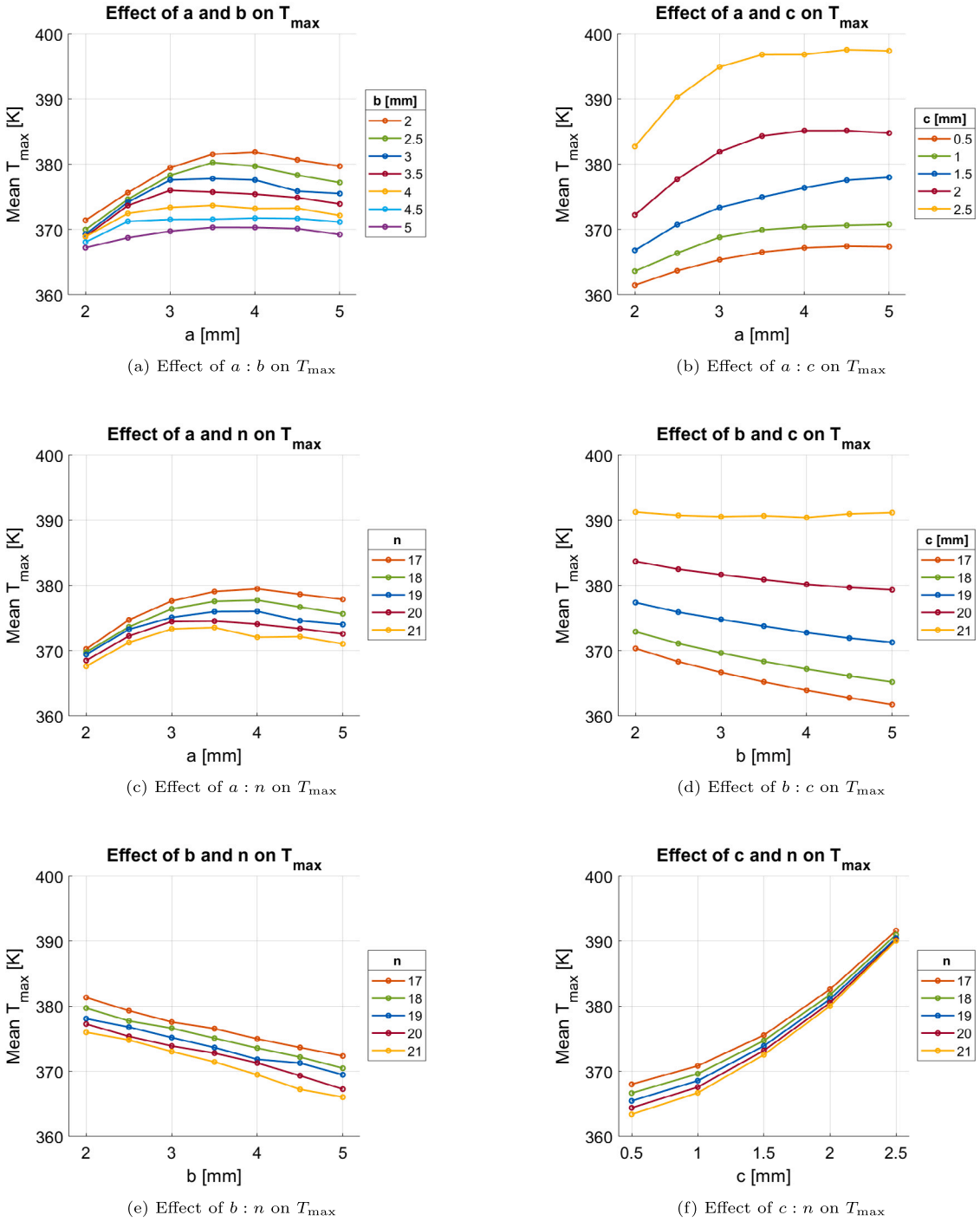

(a) Effect of $a : b$ on $T_{\max}$

(b) Effect of $a : c$ on $T_{\max}$

(c) Effect of $a : n$ on $T_{\max}$

(d) Effect of $b : c$ on $T_{\max}$

(e) Effect of $b : n$ on $T_{\max}$

(f) Effect of $c : n$ on $T_{\max}$

Fig. 10. Effects of the interactions on the maximum temperature $T_{\max}$.

Table 5
Comparison.

LCP	a [mm]	b [mm]	c [mm]	n	l [mm]	$T_{\max}$ [K]	$\lvert \nabla \mathbf{T} \rvert$ [K/m]	Δp [Pa]
Reference	3	3	1	19	4.85	365	951	1.3
Optimized	2	4	0.5	19	10.2	357	926	1.5

Regarding pressure drop (Fig. 15), the optimized LCP exhibits an average Δp of 1.5×10^3 Pa, comparable to that of the reference LCP, which is 1.3×10^3 Pa.

4. Conclusions

This study has presented a comprehensive approach for optimizing the geometric parameters of Liquid Cold Plates to enhance thermal management in railway power electronics. Through the development and application of an optimization algorithm, the objective was to minimize the maximum temperature and temperature gradient at the interface between the LCP and electronic devices. Using parametric simulation techniques and Computational Fluid Dynamics simulations with the open-source C++ toolbox OpenFOAM, the proposed methodology automates simulations and generates LCP geometries that are

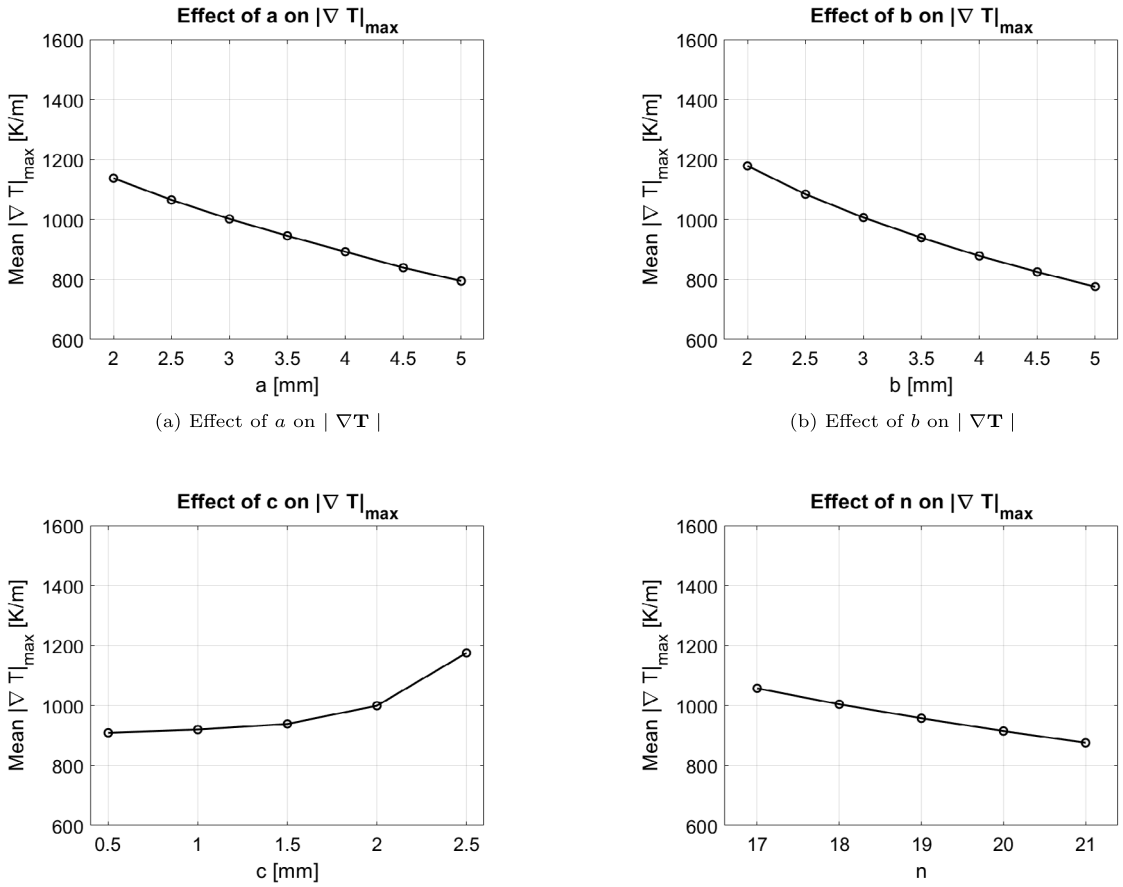

(a) Effect of a on $|\nabla \mathbf{T}|$

(b) Effect of b on $|\nabla \mathbf{T}|$

(c) Effect of c on $|\nabla \mathbf{T}|$

(d) Effect of n on $|\nabla \mathbf{T}|$

Fig. 11. Effects of single factors on magnitude of the temperature gradient $|\nabla \mathbf{T}|$.

both easy to manufacture and cost-effective, indicating the potential for real-world implementation of optimized LCP designs.

The optimization process introduced a new approach to optimize parameters, emphasizing the approximation of similar operating points rather than ensuring their exact equivalence across all Liquid Cold Plate (LCP) models. The methodology is based on the Darcy-Weisbach formula, where, once a $Q - \Delta p$ operating point is defined, the value of P/A^3 is derived. Therefore, from a computational perspective, the methodology works for any operating point and any value of P/A^3. Specifically, the predefined value of P/A^3 is satisfied through a series of independent geometric parameters (a, b, c, n) and a dependent parameter (l). While there is complete control over the independent parameters, which can thus be chosen to ensure the extrudability of the product, the same cannot be said for the dependent parameter (l) that results from them. Therefore, critical aspect of the methodology could be that, in the aftermath, it is necessary to evaluate the combinations of parameters that result in an unrealizable l. It should also be noted that, by conducting a preliminary study on the domain of the function $l = f(a, b, c, n, P/A^3)$, it is possible to ensure that the values of l are all compliant with the extrudability constraints. The study of the domain of $l = f(a, b, c, n, P/A^3)$ has not yet been integrated into the algorithm but has been conducted preliminarily in this case.

This approach enhances the reliability and applicability of optimization results in industrial contexts, providing a valuable framework for future research and development in thermal management systems. Extensive simulations and analyses conducted using the proposed algorithm showed significant reductions in computational effort, significantly reducing the time required compared to manual approaches, or saving several hours when conducting parametric studies with commercial software, but also providing significant improvements in LCP performance, including reductions in maximum interface temperature and temperature gradient. The ANOVA revealed significant influences of geometric parameters on both maximum interface temperature ($T_{\max}$) and temperature gradient (∇T) in the Liquid Cold Plate (LCP). Notably, the gap c had the most pronounced effect on $T_{\max}$, while factors a and b primarily impacted the temperature gradient. Comparison between a reference and optimized LCP showed a decrease in $T_{\max}$ in the optimized version equal to 8 K, primarily due to a reduction in c and an increase in dependent variable l.

Future developments will integrate this algorithm into a new system tailored to optimize the entire liquid thermal management system through lumped-parameter models. The new system aspires to ensure ideal operating temperatures of electronic components while minimizing energy consumption across the entire system, which includes pumps, valves, radiators, and motor-fans. This holistic approach holds promise for advancing thermal management solutions across diverse industrial applications, fostering enhanced efficiency and performance in electronic devices.

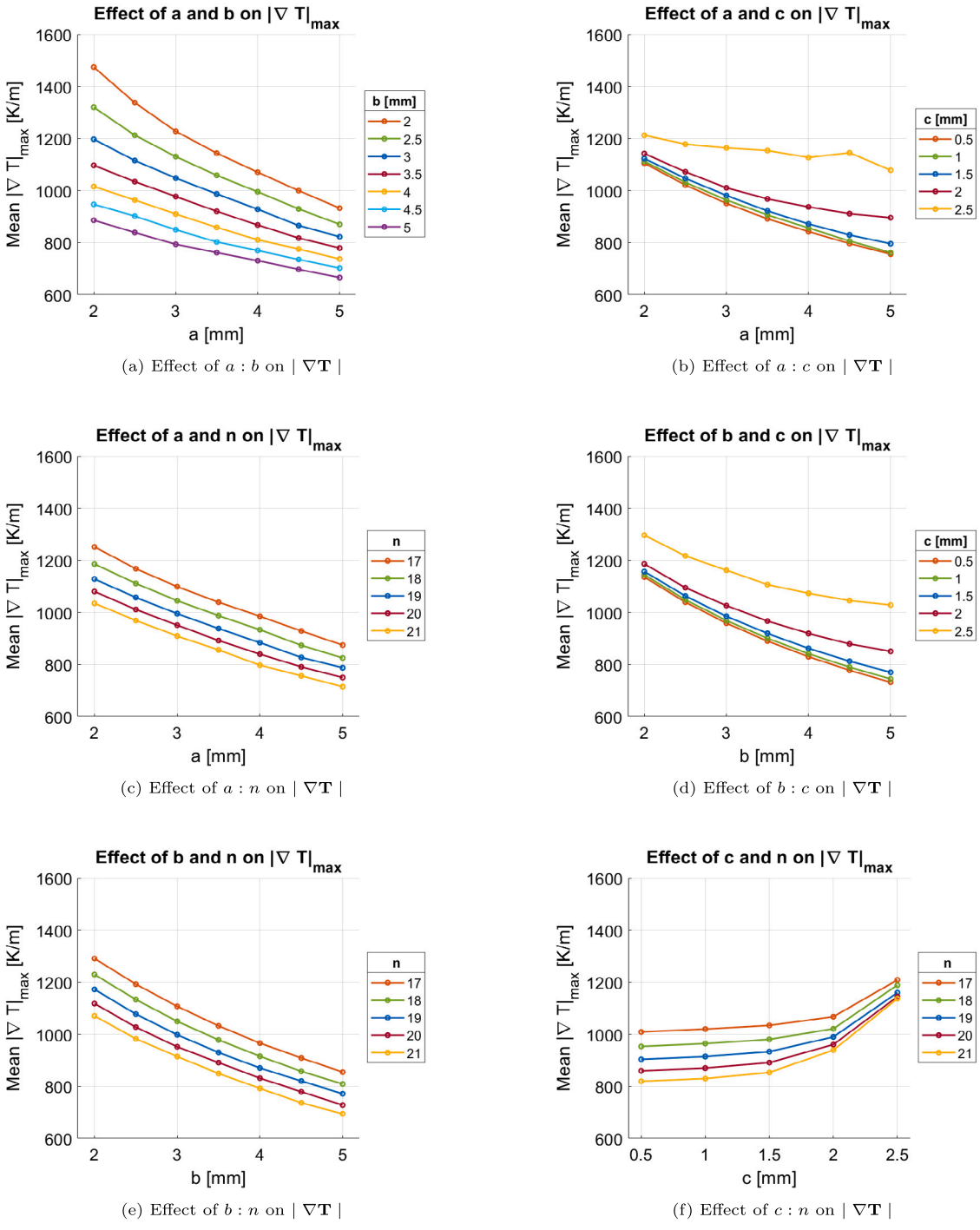

(a) Effect of $a : b$ on $|\nabla \mathbf{T}|$

(b) Effect of $a : c$ on $|\nabla \mathbf{T}|$

(c) Effect of $a : n$ on $|\nabla \mathbf{T}|$

(d) Effect of $b : c$ on $|\nabla \mathbf{T}|$

(e) Effect of $b : n$ on $|\nabla \mathbf{T}|$

(f) Effect of $c : n$ on $|\nabla \mathbf{T}|$

Fig. 12. Effects of interactions on magnitude of the temperature gradient $|\nabla \mathbf{T}|$.

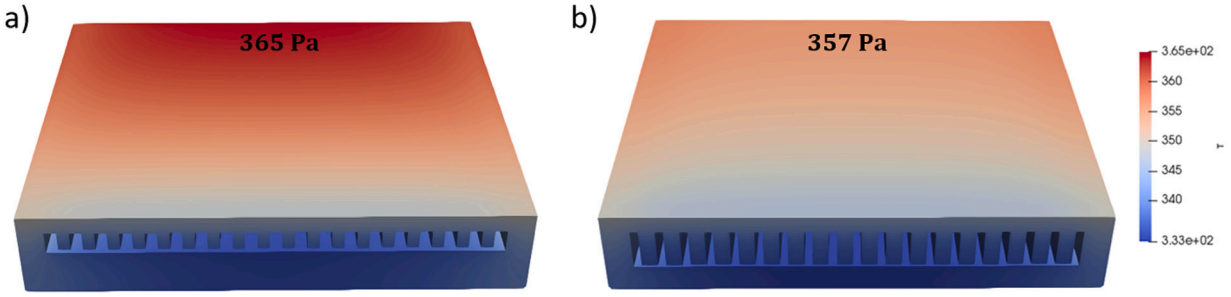

Fig. 13. Comparison between (a) the reference LCP and (b) the optimized one in terms of maximum interface temperature.

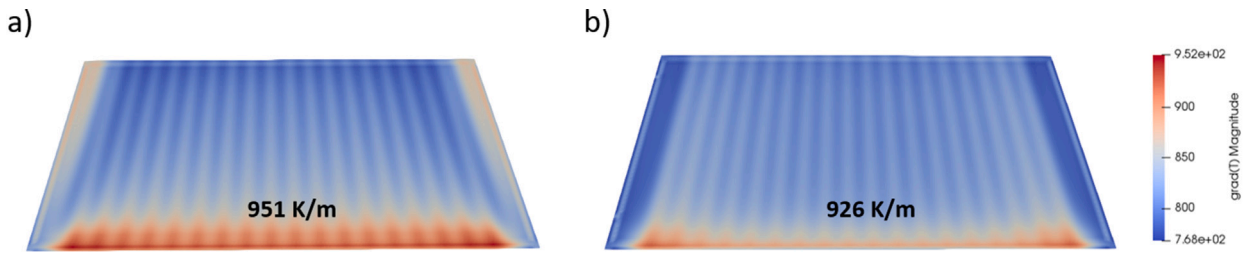

Fig. 14. Comparison between (a) the reference LCP and (b) the optimized one in terms of temperature gradient.

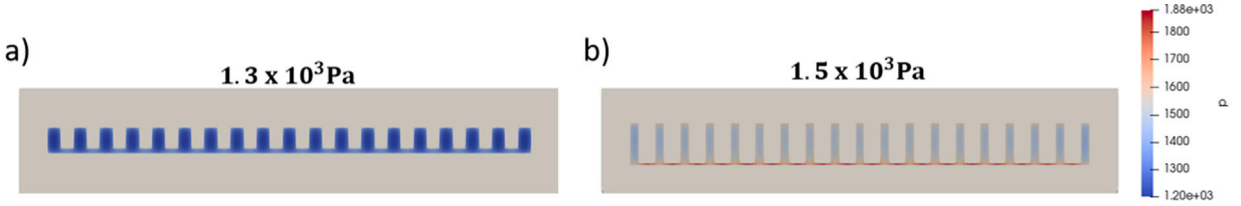

Fig. 15. Comparison between (a) the reference LCP and (b) the optimized one in terms of inlet pressure field.

CRediT authorship contribution statement

Raffaele De Rosa: Conceptualization, Methodology, Software, Formal analysis, Investigation, Data curation, Writing – original draft, Writing – review & editing, Visualization. **Marco Bernagozzi:** Validation, Resources, Writing – review & editing, Supervision. **Anastasios Georgoulas:** Validation, Resources, Writing – review & editing, Supervision. **Luca Romagnuolo:** Methodology, Data curation, Writing – review & editing, Visualization, Supervision. **Emma Frosina:** Resources, Writing – review & editing, Supervision, Project administration. **Adolfo Senatore:** Resources, Writing – review & editing, Supervision, Project administration, Funding acquisition.

Declaration of Generative AI and AI-assisted technologies in the writing process

During the preparation of this work the authors used ChatGPT 3.5 in order to improve the language. After using this tool, the authors reviewed and edited the content as needed and take full responsibility for the content of the publication.

Declaration of competing interest

The authors declare that they have no known competing financial interests or personal relationships that could have appeared to influence the work reported in this paper.

Acknowledgements

This research did not receive any specific grant from funding agencies in the public, commercial, or not-for-profit sectors.

Data availability

Data will be made available on request.

References

[1] M. Katagiri, K. Mae, Y. Nishimura, Y. Yasuda, T. Yamauchi, Development of liquid cooling system with integrated traction converters and auxiliary power supplies for 200-km/h commuter trains, 2017, URL https://www.hitachi.com/rev/archive/2017/r2017_02/10/index.html.

[2] R.D. Rosa, L. Belli, E. Frosina, P. Venanzio, L. Romagnuolo, A. Senatore, Predictive model of cooling system for railway electric propulsion: validation of design choices and last mile analysis, J. Phys. Conf. Ser. (ISSN: 1742-6596) 2385 (2022) 012062, http://dx.doi.org/10.1088/1742-6596/2385/1/012062,

[3] R.D. Rosa, L. Romagnuolo, E. Frosina, L. Belli, A. Senatore, Validation of a lumped parameter model of the battery thermal management system of a hybrid train by means of ultrasonic clamp-on flow sensor measurements and hydronic optimization, Sensors (ISSN: 1424-8220) 23 (2022) 390, http://dx.doi.org/10.3390/S23010390, 2023, Vol. 23, Page 390.

[4] X. Perpina, X. Jorda, M. Vellvehi, J. Rebollo, M. Mermet-Guyennet, Long-term reliability of railway power inverters cooled by heat-pipe-based systems, IEEE Trans. Ind. Electron. (ISSN: 02780046) 58 (2011) 2662–2672, http://dx.doi.org/10.1109/TIE.2010.2087298.

[5] S. Lohrasbi, R. Hammer, W. Essl, G. Reiss, S. Defregger, W. Sanz, A comprehensive review on the core thermal management improvement concepts in power electronics, IEEE Access (ISSN: 21693536) 8 (2020) 166880–166906, http://dx.doi.org/10.1109/ACCESS.2020.3021946.

[6] S. Mallik, N. Ekere, C. Best, R. Bhatti, Investigation of thermal management materials for automotive electronic control units, Appl. Therm. Eng. (ISSN: 1359-4311) 31 (2011) 355–362, http://dx.doi.org/10.1016/J.APPLTHERMALENG.2010.09.023.

[7] G. Moreno, Power electronics thermal management research: Annual progress report, 2017, http://dx.doi.org/10.2172/1404874.

[8] F. Hou, H. Zhang, D. Huang, J. Fan, F. Liu, T. Lin, L. Cao, X. Fan, B. Ferreira, G. Zhang, Microchannel thermal management system with two-phase flow for power electronics over 500 w/cm2heat dissipation, IEEE Trans. Power Electron. (ISSN: 19410107) 35 (2020) 10592–10600, http://dx.doi.org/10.1109/TPEL.2020.2985117.

[9] X. Cao, H. ling Liu, X. dong Shao, H. Shen, G. Xie, Thermal performance of double serpentine minichannel heat sinks: Effects of inlet-outlet arrangements and through-holes, Int. J. Heat Mass Transfer (ISSN: 0017-9310) 153 (2020) 119575, http://dx.doi.org/10.1016/J.IJHEATMASSTRANSFER.2020.119575.

[10] J. Li, W. Zuo, J. E, Y. Zhang, Q. Li, K. Sun, K. Zhou, G. Zhang, Multi-objective optimization of mini U-channel cold plate with sio2 nanofluid by RSM and NSGA-II, Energy (ISSN: 0360-5442) 242 (2022) 123039, http://dx.doi.org/10.1016/J.ENERGY.2021.123039.

[11] C.C. Wright, L.F. Wright, New, high efficiency, low cost liquid heat exchanger for cooling power semiconductor devices, in: SAE Technical Papers, 2001, http://dx.doi.org/10.4271/2001-01-1743.

[12] M.P. Bendsøe, O.O. Sigmund, Topology Optimization - Theory, Methods, and Applications, Springer Verlag, ISBN: 3-540-42992-1, 2003, p. 370.

[13] W. Wang, X. Tian, S. Qian, C. Wang, M. Wang, G. Gao, H. Liu, Secondary shape optimization of topological boundary of cold plate channels, Meccanica (ISSN: 15729648) 55 (2020) 19–33, http://dx.doi.org/10.1007/S11012-019-01108-X/FIGURES/14.

[14] F. Chen, J. Wang, X. Yang, Topology optimization design and numerical analysis on cold plates for lithium-ion battery thermal management, Int. J. Heat Mass Transfer (ISSN: 0017-9310) 183 (2022) 122087, http://dx.doi.org/10.1016/J.IJHEATMASSTRANSFER.2021.122087.

[15] C. Sun, W. Wang, X.W. Tian, X. Zeng, S.H. Qian, Y.Z. Cai, X.H. Wang, Thermal design of composite cold plates by topology optimization, Int. J. Mech. Sci. (ISSN: 0020-7403) 259 (2023) 108594, http://dx.doi.org/10.1016/J.IJMECSCI.2023.108594.

[16] S. Sun, P. Liebersbach, X. Qian, 3D Topology Optimization of Heat Sinks for Liquid Cooling, Vol. 178, 2020, 115540, http://dx.doi.org/10.1016/j.applthermaleng.2020.115540.
[17] K. Deb, A. Pratap, S. Agarwal, T. Meyarivan, A fast and elitist multiobjective genetic algorithm: NSGA-II, IEEE Trans. Evol. Comput. (ISSN: 1089778X) 6 (2002) 182–197, http://dx.doi.org/10.1109/4235.996017.
[18] A. Konak, D.W. Coit, A.E. Smith, Multi-objective optimization using genetic algorithms: A tutorial, Reliab. Eng. Syst. Saf. (ISSN: 0951-8320) 91 (2006) 992–1007, http://dx.doi.org/10.1016/J.RESS.2005.11.018.
[19] S. Bandaru, K. Deb, Multi-objective optimization, Decis. Sci. (2016) 161–200, http://dx.doi.org/10.1201/9781315183176-12, URL https://www.taylorfrancis.com/chapters/edit/10.1201/9781315183176-12/multi-objective-optimization-kalyanmoy-deb-karthik-sindhya-jussi-hakanen,
[20] Y. Cui, Z. Geng, Q. Zhu, Y. Han, Review: Multi-objective optimization methods and application in energy saving, Energy (ISSN: 0360-5442) 125 (2017) 681–704, http://dx.doi.org/10.1016/J.ENERGY.2017.02.174.
[21] X.W. Tian, S.Z. Zhang, C. Sun, W. Wang, Heat transfer enhancement in cold plates with wavy channels via free-shape modeling and optimization, Int. J. Therm. Sci. (ISSN: 1290-0729) 193 (2023) 108446, http://dx.doi.org/10.1016/J.IJTHERMALSCI.2023.108446.
[22] Y. Fan, Z. Wang, T. Fu, Multi-objective optimization design of lithium-ion battery liquid cooling plate with double-layered dendritic channels, Appl. Therm. Eng. (ISSN: 1359-4311) 199 (2021) 117541, http://dx.doi.org/10.1016/J.APPLTHERMALENG.2021.117541.
[23] L. Wei, Y. Zou, F. Cao, Z. Ma, Z. Lu, L. Jin, An optimization study on the operating parameters of liquid cold plate for battery thermal management of electric vehicles, Energies (ISSN: 1996-1073) 15 (2022) 9180, http://dx.doi.org/10.3390/EN15239180, 2022, Vol. 15, Page 9180.
[24] M. Kılıç, S. Gamsız, Z.N. Alınca, Comparative evaluation and multi-objective optimization of cold plate designed for the lithium-ion battery pack of an electrical pickup by using taguchi–grey relational analysis, Sustainability (ISSN: 2071-1050) 15 (2023) 12391, http://dx.doi.org/10.3390/SU151612391, 2023, Vol. 15, Page 12391.
[25] W. Zuo, D. Li, Q. Li, Q. Cheng, K. Zhou, J. E, Multi-objective optimization of multi-channel cold plate under intermittent pulsating flow by RSM and NSGA-II for thermal management of electric vehicle lithium-ion battery pack, Energy (ISSN: 0360-5442) 283 (2023) 129085, http://dx.doi.org/10.1016/J.ENERGY.2023.129085.
[26] J. Bies, W. Durfee, Thermal-fluid optimization of small-scale hydraulic conduits, 2022,
[27] S. Qian, W. Wang, C. Ge, S. Lou, E. Miao, B. Tang, Topology optimization of fluid flow channel in cold plate for active phased array antenna, Struct. Multidiscip. Optim. (ISSN: 16151488) 57 (2018) 2223–2232, http://dx.doi.org/10.1007/S00158-017-1852-8/TABLES/4.
[28] X.W. Tian, C. Sun, X. Zeng, S.H. Qian, C.F. Li, Y.Z. Cai, Y. Chen, W. Wang, Free-shape modeling and optimization for straight channel of cold plate involving passage pattern, cross-section, and twist of channel, Int. J. Heat Mass Transfer (ISSN: 0017-9310) 184 (2022) 122299, http://dx.doi.org/10.1016/J.IJHEATMASSTRANSFER.2021.122299.
[29] X.P. Dang, H.S. Park, Design of u-shape milled groove conformal cooling channels for plastic injection mold, Int. J. Precis. Eng. Manuf. (ISSN: 12298557) 12 (2011) 73–84, http://dx.doi.org/10.1007/S12541-011-0009-8/METRICS.
[30] Y. Hadad, N. Fallahtafti, L. Choobineh, C.H. Hoang, V. Radmard, P.R. Chiarot, B. Sammakia, Performance analysis and shape optimization of an impingement microchannel cold plate, IEEE Trans. Compon. Packag. Manuf. Technol. (ISSN: 21563985) 10 (2020) 1304–1319, http://dx.doi.org/10.1109/TCPMT.2020.3005824.
[31] Y. Hadad, B. Ramakrishnan, R. Pejman, S. Rangarajan, P.R. Chiarot, A. Pattamatta, B. Sammakia, Three-objective shape optimization and parametric study of a micro-channel heat sink with discrete non-uniform heat flux boundary conditions, Appl. Therm. Eng. (ISSN: 1359-4311) 150 (2019) 720–737, http://dx.doi.org/10.1016/J.APPLTHERMALENG.2018.12.128.
[32] M. Ahmadian-Elmi, A. Mashayekhi, S.S. Nourazar, K. Vafai, A comprehensive study on parametric optimization of the pin-fin heat sink to improve its thermal and hydraulic characteristics, Int. J. Heat Mass Transfer (ISSN: 0017-9310) 180 (2021) 121797, http://dx.doi.org/10.1016/J.IJHEATMASSTRANSFER.2021.121797.
[33] K.T. Chiang, F.P. Chang, Application of response surface methodology in the parametric optimization of a pin-fin type heat sink, Int. Commun. Heat Mass Transfer (ISSN: 0735-1933) 33 (2006) 836–845, http://dx.doi.org/10.1016/J.ICHEATMASSTRANSFER.2006.04.011.
[34] Y. Hu, Y. Joshi, Cold Plate Pin-Fin Optimization for Multi-Die Systems Using Design of Experiment, Institute of Electrical and Electronics Engineers (IEEE), 2019, pp. 991–995, http://dx.doi.org/10.1109/ITHERM.2019.8757407.
[35] S. Lee, Optimum design and selection of heat sinks, IEEE Trans. Compon. Packag. Manuf. Technol. A (ISSN: 10709886) 18 (1995) 812–817, http://dx.doi.org/10.1109/95.477468.
[36] C. Tangwongsan, Fluid velocity measurement using convective heat transfer coefficient measuring system, 2007 IEEE/NIH Life Science Systems and Applications Workshop, LISA, IEEE Computer Society, ISBN: 9781424418138, 2007, pp. 81–84, http://dx.doi.org/10.1109/LSSA.2007.4400889.
[37] J. Fernandes, S. Ghalambor, D. Agonafer, V. Kamath, R. Schmidt, Multi-design variable optimization for a fixed pumping power of a water-cooled cold plate for high power electronics applications, in: InterSociety Conference on Thermal and Thermomechanical Phenomena in Electronic Systems, ITHERM, ISBN: 9781424495320, 2012, pp. 684–692, http://dx.doi.org/10.1109/ITHERM.2012.6231494.
[38] M. Yilmaz, O. Comakli, S. Yapici, O.N. Sara, Performance evaluation criteria for heat exchangers based on first law analysis, J. Enhanced Heat Transfer (ISSN: 1065-5131) 12 (2005) 121–157, http://dx.doi.org/10.1615/JENHHEATTRANSF.V12.I2.10, URL https://www.dl.begellhouse.com/journals/4c8f5faa331b09ea,050b70ad0246b296,40dd54162c377b64.html.
[39] V. Zimparov, Extended performance evaluation criteria for enhanced heat transfer surfaces: heat transfer through ducts with constant heat flux, Int. J. Heat Mass Transfer (ISSN: 0017-9310) 44 (2001) 169–180, http://dx.doi.org/10.1016/S0017-9310(00)00074-0.
[40] V.D. Zimparov, N.L. Vulchanov, Performance evaluation criteria for enhanced heat transfer surfaces, Int. J. Heat Mass Transfer (ISSN: 00179310) 37 (1994) 1807–1816, http://dx.doi.org/10.1016/0017-9310(94)90069-8.
[41] G.O. Brown, The history of the Darcy-weisbach equation for pipe flow resistance, in: Proceedings of the Environmental and Water Resources History, American Society of Civil Engineers, ISBN: 0784406502, 2002, pp. 34–43, http://dx.doi.org/10.1061/40650(2003)4.
[42] F.M. White, H. Xue, in: M.-H. Education (Ed.), Fluid Mechanics, ISBN: 1264238495, URL https://www.mheducation.com/highered/product/fluid-mechanics-white-xue/M9781260258318.html.
[43] OpenFOAM v9 User Guide - Contents. URL https://doc.cfd.direct/openfoam/user-guide-v9/contents.
[44] ChtMultiRegionFoam - OpenFOAMWiki. URL https://openfoamwiki.net/index.php/ChtMultiRegionFoam#Equations.
[45] aov function - R Documentation. URL https://www.rdocumentation.org/packages/stats/versions/3.6.2/topics/aov.
[46] R.A. Thisted, What is a P-value, Departments of Statistics and Health Studies, 1998.
[47] D.J. Benjamin, J.O. Berger, M. Johannesson, B. A., et al., Redefine statistical significance, Nat. Hum. Behav. (ISSN: 2397-3374) 2 (2017) 6–10, http://dx.doi.org/10.1038/s41562-017-0189-z, 2017 2:1. URL https://www.nature.com/articles/s41562-017-0189-z.